Available online at www.sciencedirect.com
ScienceDirect
Journal of Power Sources 162 (2006) 713–718
JOURNAL OF POWER SOURCES
www.elsevier.com/locate/jpowsour

Crystallographic and electrochemical characteristics of icosahedral quasicrysyalline $Ti_{45-x}Zr_{35-x}Ni_{17+2x}Cu_3$ ($x = 0$–8) powders

Baozhong Liu [a,b], Yaoming Wu [a], Limin Wang [a,*]

[a] *Key Laboratory of Rare Earth Chemistry and Physics, Changchun Institute of Applied Chemistry, CAS, 5625 Renmin Street, Changchun 130022, China*
[b] *Graduate School of Chinese Academy of Science, 19 Yuquan Road, Beijing 100049, China*

Received 4 June 2006; received in revised form 17 June 2006; accepted 20 June 2006
Available online 7 August 2006

Abstract

$Ti_{45-x}Zr_{35-x}Ni_{17+2x}Cu_3$ ($x = 0$, 2, 4, 6 and 8) icosahedral quasicrystalline phase (I-phase) alloy powders are synthesized by mechanical alloying and subsequent annealing techniques, and the crystallographic and electrochemical characteristics are investigated. The alloy powders are I-phase, and the quasi-lattice constant decreases with increasing x value. The maximum discharge capacity of the I-phase alloy electrodes first increases and then decreases with increasing x value, and the $Ti_{39}Zr_{26}Ni_{29}Cu_3$ I-phase electrode exhibits the highest discharge capacity of 274 mAh g^{-1}. The high-rate dischargeability at the discharge current density of 240 mA g^{-1} increases from 55.31% ($x = 0$) to 74.24% ($x = 8$). Cycling stability also increases with increasing x value. The improvement in electrochemical characteristics may be ascribed to the added nickel, which not only improves the electrochemical activity, but also makes the alloy more resistant to oxidation.

Keywords: Ti–Zr–Ni–Cu alloy; Icosahedral quasicrystal; Exchange current density; High-rate dischargeability; Hydrogen diffusion coefficient

1. Introduction

Icosahedral quasicrystalline phase (I-phase) showing the rotational symmetry of icosahedral point group is likely dominated by local tetrahedral [1]. The dominance of polytetrahedral order makes I-phase potentially used for hydrogen storage application. Ti-base I-phase alloys are regarded as a promising hydrogen storage material due to low cost, thermodynamic stability [2,3] and high hydrogen storage capacity [4]. However, the practical application of Ti-based I-phase is inhibited by low equilibrium pressure [5] and surface barrier due to compact oxide film [6]. Some works [7,8] have been done to solve the above-mentioned problems, but it is almost impossible to desorb hydrogen at either one atmosphere pressure or room temperature. Yamaura et al. [9] have reported that very low atmospheric pressure can be obtained by the electrochemical method at room temperature. The hydride of Ti-based I-phase alloy may be dissociated in moderate condition by electrochemical method. Thus, it is very promising that Ti-based I-phase alloy is investigated as negative electrode materials of nickel–metal hydride (Ni–MH) batteries.

In our previous works, $Ti_{45}Zr_{35}Ni_{17}Cu_3$ I-phase is stable during electrochemical charging/discharging cycles [10], which indicates that it is feasible to be used as the negative electrode of Ni–MH batteries. Unfortunately, the I-phase exhibits poor electrochemical characteristics at room temperature [11]. In general, the electrochemical characteristic is related to the microstructure and the chemical composition. Jurczyk et al. [12] have reported that TiFe, $LaNi_5$ and Mg_2Ni alloys prepared by mechanical alloying and subsequent annealing exhibited excellent electrochemical hydrogen storage properties. Moreover, Kelton et al. [13] pointed out that the adsorption and desorption characteristics are improved for Ti-based I-phase alloy. In addition, metallic nickel is very good electrocatalyst and can effectively improve the charge-transfer reaction [14]. Therefore, it is expected that the electrochemical hydrogen storage characteristics should be improved for Ti–Zr–Ni–Cu I-phase with high nickel content. In present study, $Ti_{45-x}Zr_{35-x}Ni_{17+2x}Cu_3$ ($x = 0$, 2, 4, 6 and 8) alloys are synthesized by ball-milling and subsequently annealing, and electrochemical characteristics are investigated in detail.

* Corresponding author. Tel.: +86 431 526 2447; fax: +86 431 526 2447.
E-mail addresses: bzliu@ciac.jl.cn (B. Liu), lmwang@ciac.jl.cn (L. Wang).

0378-7753/$ – see front matter © 2006 Elsevier B.V. All rights reserved.
doi:10.1016/j.jpowsour.2006.06.072

2. Experimental procedures

Elemental powders of Ti (100 mesh, 99.9%), Zr (100 mesh, 99.9%), Ni (150 mesh, 99.9 %), Cu (250 mesh, 99.9%) were used as starting materials in this study. A powder mixture with a desired composition of $Ti_{45-x}Zr_{35-x}Ni_{17+2x}Cu_3$ ($x = 0$, 2, 4, 6 and 8) was poured into the milling container. Mechanical alloying (MA) was carried out in a spex800 ball miller with the protection of an argon atmosphere. The ball to powder mass ratio was 20:1, and the ball-milling time is 30 h. The powders after MA were sealed under dynamic vacuum ($<10^{-1}$ Pa) in a fused silica tube, and then annealed at 853 K for 30 min.

For electrochemical measurement, a half-cell was constructed using a $Ni(OH)_2$/NiOOH electrode as counter electrode and Hg/HgO electrode as a reference electrode in the 6 M KOH electrolyte. The charge–discharge was controlled by the potential of working electrodes, which were fabricated by compressing 0.9 g mixture of 0.15 g alloy powder and 0.75 g Ni carbonyl powder into a pellet of 10 mm diameter under a pressure of 15 MPa, with respect to the reference electrode with on automatic galvanostatic charge–discharge apparatus (DC-5). The electrode was charged at 60 mA g^{-1} for 7 h and discharged at 30 mA g^{-1} to the cut-off voltage of –0.6 V (versus Hg/HgO). After every charging/discharging, the rest time was 5 min. In evaluating the high rate dischargeability, discharge capacity of the alloy electrode at different discharge current density were measured. The high-rate dischargeability HRD (%) defined as $C_n \times 100/(C_n + C_{30})$, was determined from the ratio of the discharge capacity C_n ($n = 60$, 90,120, 180 and 240, respectively) to the total discharge capacity defined as the sum of C_n and C_{30}, which was additional capacity measured subsequently at 30 mA g^{-1} after C_n was measured.

The phase compositions and microstructures were also characterized by X-ray diffraction (XRD) and transmission electron microscope (TEM). The electrochemical impedance spectroscopy (EIS) analysis was carried out on a Solartron 1287 Potentiostat/Galvanostat and a Solartron 1255 frequency response analyzer with Z-POLT software for WINDOWS. The electrodes were all tested at 10% depth of discharge (DOD) at the fifth cycle, and the frequency range was from 0.1 Hz to 1 MHz. The potentiostatic discharge technique was used to evaluate the diffusion coefficient of hydrogen in the bulk of the alloy. After being fully charged followed by 30 min open-circuit lay-aside, the test electrodes were discharged with +500 mV potential-step for 3000 s on the EG&G PARC Model 273Potentiostatic/Galvanostat, using the M352 corrosion software.

3. Results and discussion

3.1. Phase structure

Fig. 1 shows XRD patterns of $Ti_{45-x}Zr_{35-x}Ni_{17+2x}Cu_3$ alloy powders. It can be seen that all alloy powders exhibit the diffraction peaks corresponding to I-phase. The prominent I-phase is indexed following the scheme originally proposed by Bancel et al. [15]. The peaks shift to larger angle with increasing x value, which implies quasi-lattice constant of I-phase becomes smaller. According to report [16], the quasi-lattice constants (a_Q) of the I-phase alloys are calculated and listed in Table 1. The a_Q decreases from 5.173 Å ($x = 0$) to 5.093 Å ($x = 8$). Fig. 2 shows bright-field TEM image and selected diffraction pattern of the $Ti_{39}Zr_{29}Ni_{29}Cu_3$ alloy powder. The particles in the diameter range below 80 nm are seen over whole area for the powder. The selected diffraction pattern (b) is identified as I-phase. Considering the XRD results, it is concluded that the $Ti_{39}Zr_{29}Ni_{29}Cu_3$ alloy powder is an I-phase.

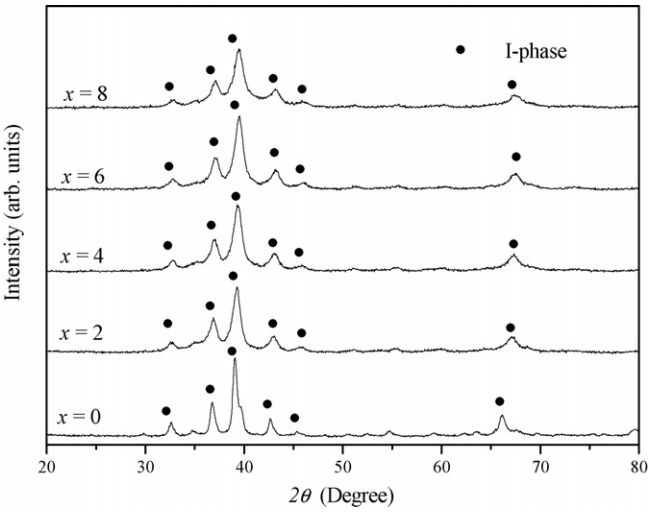

Fig. 1. XRD patterns of $Ti_{45-x}Zr_{35-x}Ni_{17+2x}Cu_3$ alloy powders.

3.2. Maximum discharge capacity and activation property

The numbers of cycles needed to activate the electrodes are given in Table 1. It is noted that all the alloy electrodes can be activated at two charging/discharging cycles. This indicates that I-phase alloys exhibit excellent activation property. The maximum discharge capacities of the I-phase alloy electrodes are also presented in Table 1. It can be seen that the maximum discharge capacities have a maximum value with increasing Ni content, namely, the $Ti_{39}Zr_{29}Ni_{29}Cu_3$ I-phase alloy has the highest discharge capacity of 274 mAh g^{-1}. As our previous reported [10,11], the low discharge capacity of the $Ti_{45}Zr_{38}Ni_{17}Cu_3$ I-phase alloy electrode was ascribed to the high stability and poor electrochemical kinetics. Gao et al. [17] have reported the stability of alloy hydride decreased with the increase of instable hydride elements. The larger content of Ni addition can decrease

Table 1
Quasi-lattice constant and electrode performance of I-phase alloy electrodes

Sample	a_Q (Å)	C_{max} (mAh g^{-1})	HRD (%)[a]	N_a[b]	S_{15} (%)
$x = 0$	5.173	143	55.31	2	57.3
$x = 2$	5.134	202	56.05	1	57.9
$x = 4$	5.126	235	57.61	1	61.7
$x = 6$	5.104	274	61.47	1	63.6
$x = 8$	5.093	269	74.24	1	76.9

[a] The high-rate dischargeability at the discharge current density of 240 mA g^{-1}.
[b] The number of cycles needed to activate the electrodes.

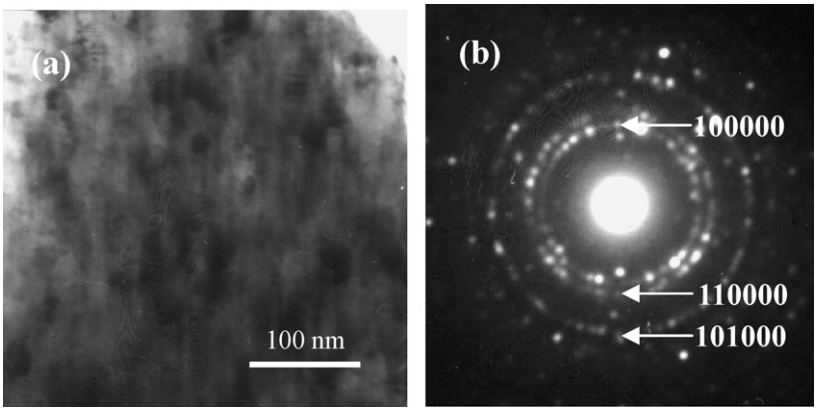

Fig. 2. TEM image and selected diffraction pattern of the $Ti_{39}Zr_{29}Ni_{29}Cu_3$ alloy powder. (a) Bright-field; (b) selected diffraction pattern.

the stability to a larger extent, and contributes to enhancing the discharge capacity of the $LaMg_{12}$ alloy. The bond strength of Ni–H is weaker than that of Ti–H and Zr–H. The increase of Ni content will decrease the stability of Ti–Zr–Ni–Cu alloy hydride. Ovshinsky et al. [18] have reported the combination of Ni with Ti or Zr contributes to the resistance of the alloy to oxidation and produces oxide films at the electrode/electrolyte interface that contain metallic region, which help provide the electrical conductivity and catalytic activity. Increasing Ni content at the surface contributes to the improvement of the charge-transfer reaction and makes the hydrogen diffusion more easily through the electrode/electrolyte interface. On the other hand, Brateng et al. [19] pointed out that discharge capacity has a linear relationship with the cell volume. The less the cell volume is, the less the discharge capacity. The decrease of quasi-lattice constant is detrimental to the discharge capacity. Takasaki and Kelton [20] have investigated the thermal desorption of hydrogen for Ti–Zr–Ni I-phase alloy, and pointed out that the decrease of the quasi-lattice content strengthens the physical interaction between the hydrogen and the neighboring metal atoms. The decrease of quasi-lattice constant will cause hydrogen diffusion in the bulk alloy more difficult. Obviously, the decrease of the hydride stability and the improvement of electrochemical kinetics resulted from the increase of Ni content are favorable for the maximum discharge capacity, but the decrease of quasi-lattice constant is unfavorable. Therefore, it is reasonable to assume that, with Ni content of lower than a certain amount, the favorable effect of Ni is dominant and will cause an increase of the maximum discharge capacity. However, when Ni content exceeds the critical content, the unfavorable effect will become dominant and will give rise to the decrease of the maximum discharge capacity. The critical content amount of Ni addition is $x = 6$ for the $Ti_{45-x}Zr_{35-x}Ni_{17+2x}Cu_3$ I-phase alloys.

3.3. High-rate dischargeability (HRD) and electrochemical kinetics

As an important kinetics property of the hydride electrode in battery, it is very important to minimize the decrease in discharge capacity even at the high discharge current density [21]. Fig. 3 shows the relationship between the high-rate dischargeability and the discharge current density of $Ti_{45-x}Zr_{35-x}Ni_{17+2x}Cu_3$ I-phase alloy electrodes. The HRD of the alloy electrodes increases with the increase of x value. The HRD at the discharge current density of 240 mA g^{-1} is also listed in Table 1. It can be seen that HRD increases from 55.31% ($x = 0$) to 74.24% ($x = 8$). It is well known that the HRD of the metal-hydride electrodes is dominated by the electrochemical kinetics of the charge-transfer reaction at the electrode/electrolyte interface and the hydrogen diffusion rate within the bulky alloy electrode, which are reflected in the value of the charge-transfer resistance (R_{ct}) and/or surface exchange current density (I_0), being a measure of the catalytic activity of an alloy, as well as in the hydrogen diffusion coefficient (D), which characterizes the mass transport properties of an alloy electrode [22]. In order to examine the electrochemical kinetic properties, electrochemical impedance and potential-step experiment are performed on the investigated I-phase alloy electrodes.

Fig. 4 shows the EIS of the I-phase alloy electrodes at 10% DOD at the fifth cycle and their equivalent circuit. On the basis of the circuit and by means of fitting program Z-VIEW, R_{ct} are obtained. Table 2 gives R_{ct} and I_0 obtained by the following

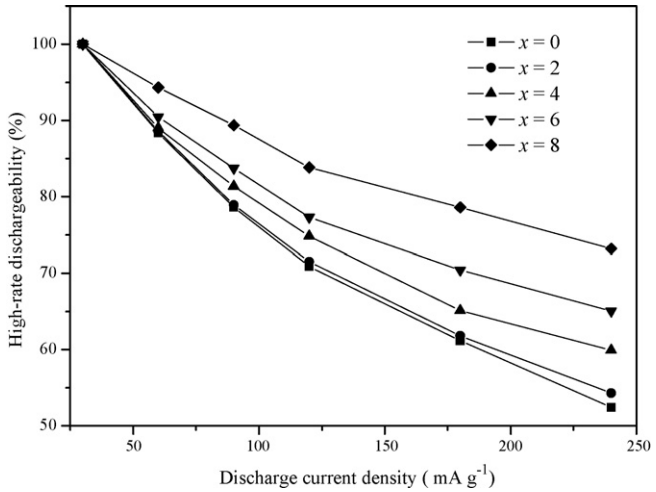

Fig. 3. High-rate dischargeability of $Ti_{45-x}Zr_{35-x}Ni_{17+2x}Cu_3$ I-phase alloy electrodes.

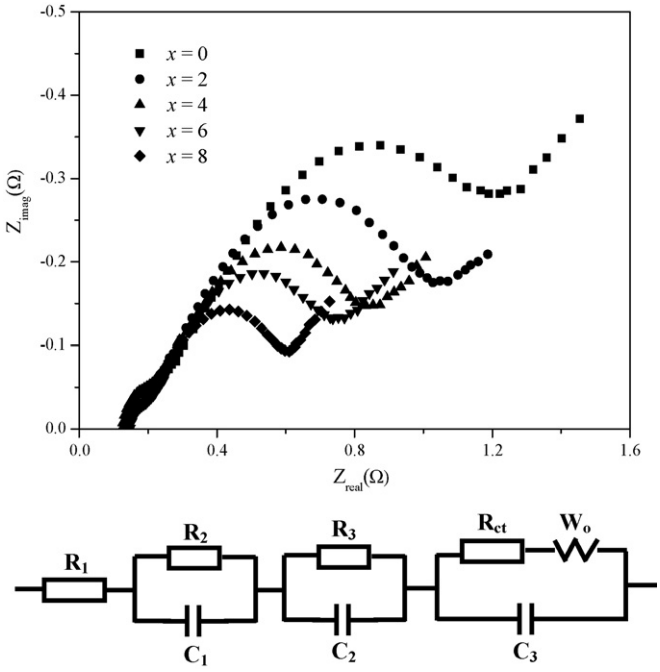

Fig. 4. EIS of $Ti_{45-x}Zr_{35-x}Ni_{17+2x}Cu_3$ I-phase alloy electrodes at 10% DOD and their equivalent circuit.

equation assuming the surface state of the alloy electrodes is same [23]:

$$I_0 = \left(\frac{RT}{F}\right)\left(\frac{1}{R_{ct}}\right)$$

where R is the gas constant, T the absolute temperature and F is the Faraday constant. It is clear that the R_{ct} decreases and I_0 increases with increasing x value. The calculated results show that the R_{ct} of $Ti_{45-x}Zr_{35-x}Ni_{17+2x}Cu_3$ I-phase alloy electrode decreases from 139.5 mΩ g ($x=0$) to 57.9 mΩ g ($x=8$), and accordingly the I_0 increases from 199.5 mA g^{-1} ($x=0$) to 480.7 mA g^{-1} ($x=8$). It is well known that metallic nickel is very good electrocatalyst and very important to improve the electrochemical kinetics at the electrode/electrolyte interface. The improvement of the charge-transfer reactions, namely the decrease of the charge-transfer resistance and the increase of the exchange current density, is ascribed to the increasing Ni content at the surface.

The diffusion coefficient of hydrogen in the I-phase alloy electrodes is determined with the potential-step method. Fig. 5 shows the semi-logarithmic plots of the anodic current versus the time response. According to the model [24] and assuming that the alloy electrodes have a similar particle distribution with an average particle radius of 5 μm. The hydrogen diffusion coefficient D in the bulk of alloy electrodes is estimated and also listed in Table 2. The D of $Ti_{45-x}Zr_{35-x}Ni_{17+2x}Cu_3$ I-phase alloy electrodes increases from 5.8×10^{-10} cm^2 s^{-1} ($x=0$) to 10.5×10^{-10} cm^2 s^{-1} ($x=8$). As mentioned above, the increase of Ni content produces more metal region at the electrode/electrolyte interface, which helps provide the electrical conductivity and catalytic activity so that the hydrogen atoms diffuse through the surface oxide films more easily. Unfortunately, increasing nickel content leads to the decrease of the quasi-lattice constant, and then strengthens the physical interaction between the hydrogen and the neighboring metal atoms, which is unfavorable for the hydrogen diffusion in the bulk I-phase electrodes. Therefore, it is reasonable to assume that the hydrogen diffusion through the surface oxide films is more important for the I-phase alloy electrodes in present work.

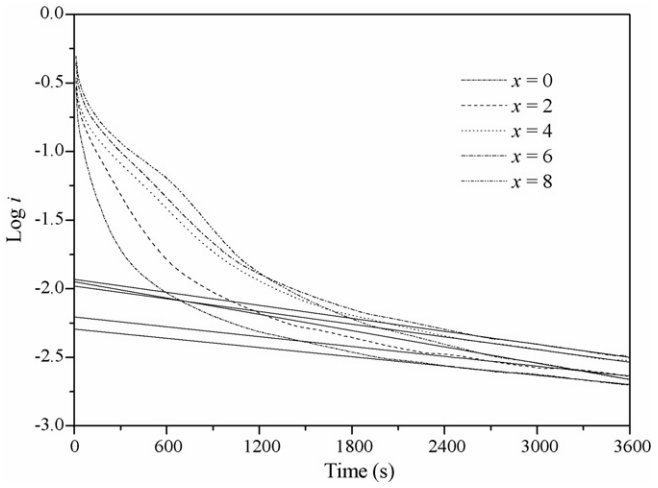

Fig. 5. Anodic current–time responses of $Ti_{45-x}Zr_{35-x}Ni_{17+2x}Cu_3$ I-phase alloy electrodes.

Table 2
Electrochemical kinetic parameters of $Ti_{45-x}Zr_{35-x}Ni_{17+2x}Cu_3$ I-phase alloy electrodes

Sample	R_{ct} (mΩ g)	I_0 (mA g^{-1})	D ($\times10^{-10}$ cm^2 s^{-1})
$x=0$	139.5	199.5	5.8
$x=2$	121.5	229.1	6.3
$x=4$	92.4	301.2	7.4
$x=6$	71.2	390.9	8.4
$x=8$	57.9	480.7	10.5

Iwakura et al. [25,26] have reported that if the electrochemical kinetics at the electrode/electrolyte interface is rate-determine, a linear dependence of the high-rate dischargeability on the exchange current density should be observed. In contrast, if the diffusion of hydrogen in the bulk I-phase alloy is rate-determine, a linear dependence of the high-rate dischargeability on the hydrogen diffusion coefficient should be found. As shown in Fig. 6, it is clear that the HRD at the current density of 240 mA g^{-1} increases with the increase of the exchange current density and hydrogen diffusion coefficient. The linear dependence of the high-rate dischargeability on both the exchange current density and the hydrogen diffusion coefficient can be observed, which implies that both charge-transfer reaction at the electrode/electrolyte interface and the hydrogen diffusion in the bulk I-phase alloy electrode should be responsible for the improvement of high-rate dischargeability in present work.

3.4. Cycling stability

Fig. 7 shows discharge capacities as a function of cycle number for the I-phase alloy electrodes. It can be noted that

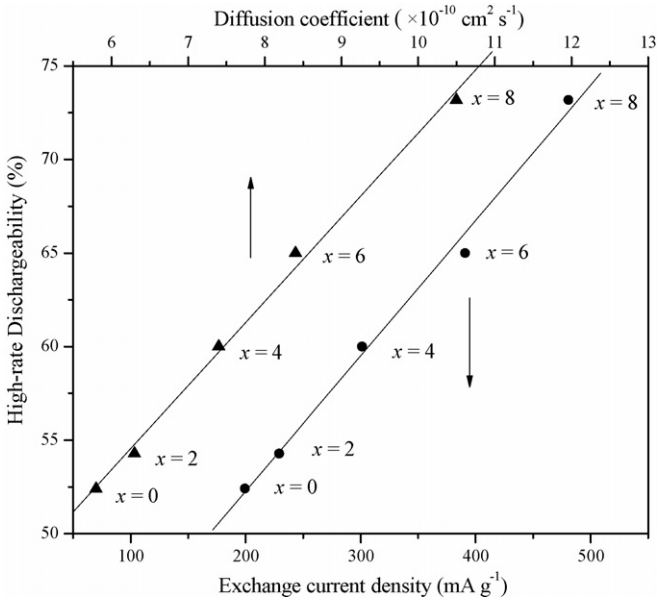

Fig. 6. HRD at 240 mA g^{-1} as a function of exchange current density and hydrogen diffusion coefficient for $Ti_{45-x}Zr_{35-x}Ni_{17+2x}Cu_3$ I-phase alloy electrodes.

increasing nickel content obviously improves cycling stability. After 15 cycles, the discharge capacity of the $Ti_{37}Zr_{27}Ni_{34}Cu_3$ I-phase alloy electrode is 207 mAh g^{-1}, which is 2.5 times higher than that of $Ti_{45}Zr_{35}Ni_{17}Cu_3$ electrode. The cycling capacity retention rate, expressed as S_{15} (%) = $C_{15}/C_{max} \times 100$ (where C_{max} is the maximum discharge capacity, C_{15} is the discharge capacity at the 15th cycle), is listed in Table 1. The calculated results of $Ti_{45-x}Zr_{35-x}Ni_{17+2x}Cu_3$ I-phase alloy electrodes show S_{15} increases noticeable from 57.3% to 76.9% with increasing x value from 0 to 8. As reported previously [27,28], the formation of passive layer of Ti and Zr on the alloy surface is ascribed as the main cause of cycling capacity degradation, because such a layer decreases the electrochemical kinetic and the electronic conductivity, and thus reduces discharge capacity of Ti/Zr-based alloy electrodes. It is well known that metallic nickel is resistant to oxidation in alkali solution. Metallic nickel at the surface oxide films will increase with increasing x value. Metallic nickel at the surface not only plays a catalyst role in the electrode reaction, but also raises the electronic conductivity. It can be believed the improvement of cycling stability is ascribed to the increasing nickel content in the alloys.

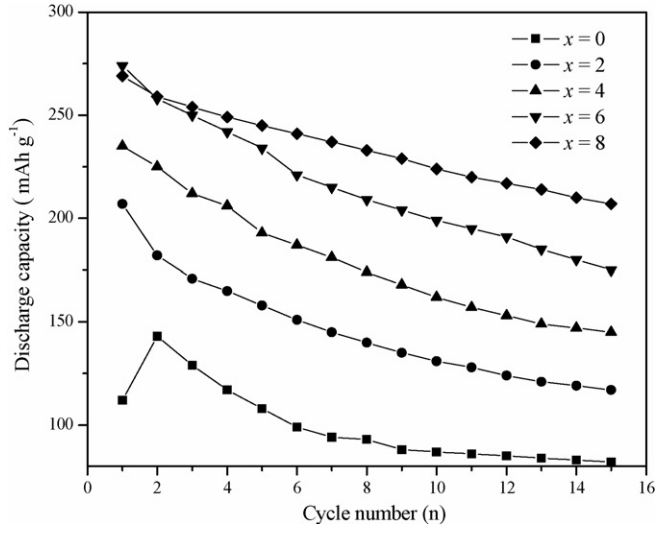

Fig. 7. Discharge capacities as a function of cycle number for $Ti_{45-x}Zr_{35-x}Ni_{17+2x}Cu_3$ I-phase alloy electrodes.

4. Conclusions

$Ti_{45-x}Zr_{35-x}Ni_{17+2x}Cu_3$ (x = 0, 2, 4, 6 and 8) I-phase powders are synthesized successfully by using mechanical alloying and subsequent annealing techniques. The quasi-lattice constant (a_Q) of the I-phase decreases from 5.173 Å (x = 0) to 5.093 Å (x = 8). The maximum discharge capacity of I-phase alloy electrodes first increases form 143 mAh g^{-1} (x = 0) to 273 mAh g^{-1} (x = 6), and then decreases to 269 mAh g^{-1} (x = 8). The HRD at the discharge current density of 240 mA g^{-1} increases from 55.31% (x = 0) to 74.24% (x = 8) and is under combined control of the electrochemical kinetics and the hydrogen diffusion. In addition, cycling stability is also improved and S_{15} increases noticeable from 57.3% (x = 0) to 76.9% (x = 8). The improvement in electrochemical property should be ascribed to the increasing nickel content, which improves the electrochemical kinetic properties and prevents the oxidation of the alloy electrodes.

Acknowledgments

This work is supported by National Natural Science Foundations of China (50571094) and Chinese Academy of Science for Distinguished Talents Program. The authors would like to thank Mr. Jianli Wang, Qiuming Peng and Wenya Yin for helpful work.

References

[1] A.M. Viano, R.M. Stroud, P.C. Gibbons, A.F. Mcdowell, M.S. Conradi, K.F. Kelton, Phys. Rev. B 51 (1995) 12026–12029.
[2] K.F. Kelton, W.J. Kim, R.M. Stroud, Appl. Phys. Lett. 70 (1997) 3230–3232.
[3] R.G. Hennig, A.E. Carlsson, K.F. Kelton, C.L. Henley, Phys. Rev. B 71 (2005) 144103–144110.
[4] R.M. Stroud, A.M. Viano, P.C. Gibbons, K.F. Kelton, S.T. Misture, Appl. Phys. Lett. 69 (1996) 2998–3000.
[5] K.F. Kelton, Mater. Sci. Eng. A 375 (2004) 31–37.
[6] A.M. Viano, E.H. Majzoub, R.M. Stroud, M.J. Kramer, S.T. Misture, P.C. Gibbons, K.F. Kelton, Phil. Mag. A 78 (1998) 131–141.
[7] J.Y. Kim, P.C. Gibbons, K.F. Kelton, J. Alloys Compd. 266 (1998) 311–317.
[8] A. Takasaki, K.F. Kelton, J. Alloys Compd. 347 (2002) 295–300.
[9] S.I. Yamaura, H.Y. Kim, H. Kimura, A. Inoue, Y. Arata, J. Alloys Compd. 329 (2002) 230–235.
[10] B.Z. Liu, Y.M. Wu, L.M. Wang, J. Power Sources, in press.
[11] B.Z. Liu, Y.M. Wu, L.M. Wang, Int. J. Hydrogen Energy 31 (2006) 1394–1400.
[12] M. Jurczyk, L. Smardz, A. Szajek, Mater. Sci. Eng. B 108 (2004) 67–75.
[13] K.F. Kelton, J.J. Hartzell, R.G. Hennig, V.T. Huett, A. Takasaki, Phil. Mag. 86 (2006) 957–964.
[14] Y.H. Xu, C.P. Chen, X.L. Wang, Q.D. Wang, Solid State Ionics 146 (2002) 157–161.
[15] P. Bancel, P. Heiney, P. Stephens, A. Goldman, P. Horn, Phys. Rev. Lett. 54 (1985) 2422–2425.

[16] C.L. Henley, V. Elser, Phil. Mag. B 53 (1986) L59–L66.
[17] X.P. Gao, Y. Wang, Z.W. Lu, F. Wu, D.Y. Song, P.W. Shen, Chem. Mater. 16 (2004) 2515–2517.
[18] S.R. Ovshinsky, M.A. Fetcenko, J. Ross, Science 260 (1993) 176–181.
[19] R. Brateng, S. Gulbrandsen-Dahl, L.O. Vaøen, J.K. Solberg, R. Tunold, J. Alloys Compd. 396 (2005) 100–107.
[20] A. Takasaki, K.F. Kelton, Int. J. Hydrogen Energy 31 (2006) 183–190.
[21] X.B. Zhang, D.Z. Sun, W.Y. Yin, Y.J. Chai, M.S. Zhao, Chem. Phys. Chem. 6 (2005) 520–525.
[22] Y.F. Liu, H.G. Pan, M.X. Gao, R. Li, Y.Q. Lei, J. Alloys Compd. 376 (2004) 304–311.
[23] N. Kuriyama, T. Sakai, H. Miyamura, I. Uehara, H. Ishikawa, J. Alloys Compd. 202 (1993) 183–197.
[24] G. zheng, B.N. Popov, R.E. White, J. Electrochem. Soc. 142 (1995) 2695–2698.
[25] C. Iwakura, M. Miyamoto, H. Inoue, M. Matsuoka, Y. Fukumoto, J. Alloys Compd. 259 (1997) 132–134.
[26] C. Iwakura, T. Oura, H. Inoue, M. Matsuoka, Electrochim. Acta 41 (1995) 117–121.
[27] H.H. Lee, K.Y. Lee, J.Y. Lee, J. Alloys Compd. 253–254 (1997) 601–604.
[28] X.B. Yu, Z. Wu, B.J. Xia, N.X. Xu, J. Chem. Phys. 121 (2004) 987–990.